

An Internal ALD-Based High Voltage Divider and Signal Circuit for MCP-based Photodetectors

Bernhard Adams^b, Andrey Elagin^a, Jeffrey W. Elam^b, Henry J. Frisch^a,
Jean-Francois Genat^{a,1}, Joseph S. Gregar^b, Anil U. Mane^b, Michael J. Minot^c,
Richard Northrop^a, Razib Obaid^{a,2}, Eric Oberla^a, Alexander Vostrikov^a,
Matthew Wetstein^a

^a*Enrico Fermi Institute, University of Chicago*

^b*Argonne National Laboratory*

^c*Minotech Engineering, Inc and Incom, Inc*

Abstract

We describe a pin-less design for the high voltage (HV) resistive divider of the all-glass LAPPDTM 8"-square thin photodetector module. The divider, which distributes high voltage applied to the photocathode to the two micro-channel plates (MCP's) that constitute the amplification stage, is comprised of the two MCP's and three glass mechanical spacers, each of which is coated with a resistive layer using Atomic Layer Deposition (ALD). The three glass grid spacers and the two MCP's form a continuous resistive path between cathode and anode, with the voltages across the MCP's and the spacers determined by the resistance of each. High voltage is applied on an external tab on the top glass window that connects to the photocathode through the metal seal. The DC ground is supplied by microstrips on the bottom glass plate that form the high-bandwidth anode. The microstrips exit the package through the glass-frit seal of the anode base-plate and the package sidewall. The divider is thus completely internal, with no HV pins penetrating the low-profile flat glass package. Measurements of the performance of the divider are presented for the 8"-square MCP and spacer package in a custom test fixture and for an assembled externally-pumped LAPPDTM prototype with an aluminum photocathode.

¹Present address, Universit  s Pierre et Marie Curie; Paris France

²Present address, Physics Dept., Univ. of Conn., Storrs, CT 06269

11	Contents	
12	1 Introduction	3
13	2 The HV Resistive Distribution Chain	5
14	2.1 Resistive Components	6
15	2.2 DC Current Path	8
16	2.3 The Signal Path for Fast-Risetime Pulses	10
17	2.3.1 Normal Anode Configuration	11
18	2.3.2 The ‘Inside-Out’ Anode	12
19	3 Implementation in the LAPPDTM Package	14
20	3.1 Mechanical Dimensions	14
21	4 Performance of the HV Divider	16
22	4.1 Test Facilities	17
23	4.1.1 The Spacer Station (ISS)	17
24	4.1.2 The Demountable Tile	17
25	4.2 Current-vs-Voltage (I-V) Curves	20
26	4.3 Thermal Coefficient	20
27	4.4 Pressure Dependence	21
28	4.5 Long-term Stability	22
29	5 Conclusions	23
30	6 Acknowledgments	24

1. Introduction

The LAPPD Collaboration [1] was formed to develop large-area photodetectors based on micro-channel plates [2] for precise time-of-flight measurements in large-scale detectors for High Energy Physics. In a number of applications the ability to detect the arrival of multiple photons in a large-area plane, each measured with a time resolution measured in pico-seconds ($1 \text{ psec} = 10^{-12} \text{ sec}$) and a space resolution measured in millimeters, enables a 3D pattern reconstruction using the 2D position of arrival of each photon and the transit time to determine the remaining orthogonal 3rd component [3]. Additionally, a psec-level measurement of the time coordinate allows a qualitative change in the photodetector area needed to provide a given level of coverage for large diffuse sources such as the large water-Cherenkov or scintillation counters used in particle and nuclear physics, as the addition of the transit drift time of the photon transforms a 2-dimensional phase space into a much larger 3-dimensional space. Optical systems can take advantage of measuring both the position and the time of arrival to minimize expensive photocathode area while still preserving space resolution³.

The amplification in conventional discrete-dynode photomultipliers (PMT's) and microchannel-based photomultipliers (MCP-PMT's) is done by electron multiplication, with the electrons accelerated between collisions with a dynode (in a PMT) or the wall of a capillary channel (in an MCP-PMT) to provide energy for secondary electron emission. The multiplication is consequently exponential, and depends on the secondary-emission yield (SEY) of each collision and the number of collisions (equal to the number of dynodes in a PMT). The SEY in turns depends on the accelerating voltage between collisions, which in a PMT is typically set by a resistive voltage divider that supplies each dynode from a high voltage (HV) source at the input to the divider. The principle is the

³One can think of this as similar to rotations between transverse and longitudinal emittances in accelerators.

58 same in an MCP-PMT, but rather than a divider made of discrete resistive ele-
 59 ments, the voltages between collisions are set by a DC current flowing through a
 60 resistive layer on the walls of the capillaries. In an MCP-PMT with the typical
 61 pair of capillary plates as an amplification section, voltage is usually applied
 62 to the top and bottom of each plate by deposition of a conducting electrode
 63 surface.

64 The LAPPDTM (Large Area Picosecond Photodetector) is an MCP-based
 65 photodetector, capable of imaging at high spatial and temporal resolution, in an
 66 ultra-high vacuum (UHV) hermetic package with an active area of 400 square
 67 centimeters. The modular detector design is based on a hermetic all-glass vac-
 68 uum tube package consisting of a thin window on which a bialkali photocathode
 69 has been deposited, two 8"-square micro-channel plates (MCP), and an anode
 70 implemented as high-bandwidth RF silver micro-striplines [4]. Amplification is
 71 provided by a pair of micro-channel glass substrates [5] coated by Atomic Layer
 72 Deposition (ALD) [6], with typical gains of more than 10^7 .

73 The HV distribution for the LAPPDTM can be implemented in a number of
 74 ways, depending on the application and possibly also on parameters of the pro-
 75 duction process. In the design described here, the HV distribution and the high
 76 frequency signal path are both integral parts of an economical mechanical struc-
 77 ture. The hermetic package has only 8 parts, all made of commonly-available
 78 sheet glass. The only additional element is a simple getter assembly formed
 79 from a strip of getter material and glass bead supports that is situated around
 80 the circumference of the channel plate stack assembly. An attractive feature
 81 for robustness and fabrication yield is there are no pins penetrating the pack-
 82 age; both the HV and the anode signals are brought in through metal layers
 83 deposited on the glass prior to assembly. The planar anode signal plane has an
 84 analog bandwidth of 1.6 GHz (3 db loss) [4] in this implementation.

85 The organization of the paper is as follows. Section 2 describes the resistive
 86 HV distribution chain, with the resistive elements and DC current path de-
 87 scribed in Sections 2.1 and 2.2, respectively. The high-speed (radio-frequency,
 88 RF) signal circuit, which is electrically and mechanically integrated with the

89 HV circuit, is discussed in Section 2.3 for the usual configuration with the an-
90 ode pattern on the inside surface of the vacuum volume (Section 2.3.1), and a
91 capacitively-coupled configuration with pads or microstrips on the outside sur-
92 face (Section 2.3.2). The integration of the HV divider into the LAPPDTM her-
93 metic package is described in Section 3, where the physical dimensions, ALD
94 coating parameters, and electrical values are also summarized.

95 Measurements of the performance of the HV divider are presented in Sec-
96 tion 4. A summary of the test facilities for the HV chain is given in Sec-
97 tion 4.1. Section 4.1.1 describes a custom test facility, the Spacer Station (ISS),
98 used to make DC measurements of current and voltage. A second test facility,
99 the ‘Demountable Tile’, consisting of an LAPPDTM glass-body tile mechanical
100 assembly, but with an O-ring window seal and a permanent connection to a
101 vacuum pump rather than being a hermetically sealed tube, is used to make
102 measurements of fast pulses, including time and space resolutions, as described
103 in Section 4.1.2. Measurements of I-V curves and the dependence of the divider
104 resistance on temperature, pressure, and time are presented in Sections 4.2-4.5.
105 The paper concludes with a summary in Section 5.

106 **2. The HV Resistive Distribution Chain**

107 The hermetic package, made of readily-available borosilicate glass [7], con-
108 sists of a top window, sidewall, and anode bottom plate. The sidewall is her-
109 metically sealed to the anode plate with glass frit to form a robust base unit.
110 The top window is sealed with indium to the base in vacuum after the photo-
111 cathode is deposited. HV is applied outside the vacuum volume on a window
112 tab that makes contact with the metalized border of the window and the photo-
113 cathode. Resistive grid spacers coated by ALD support the pressure on the top
114 window and bottom anode plate. The three spacers and the two MCP plates,
115 together with the (DC) grounded anode plane, form the resistive HV divider
116 that determines the voltages across the MCP’s and the three gaps. The silver
117 anode strips [8] extend beyond the sidewall bottom seal to complete the electri-

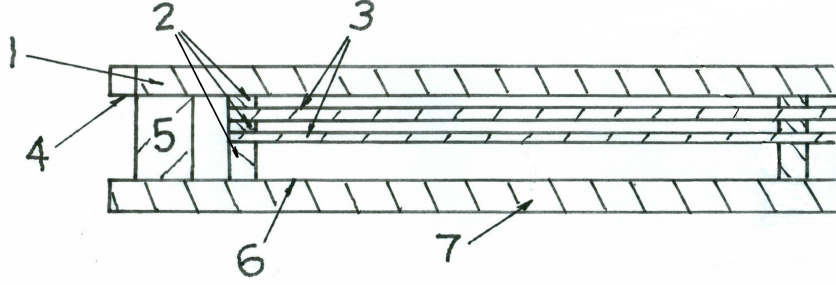


Figure 1: The mechanical construction of the LAPPDTM module. All components are glass. The hermetic volume is formed by the top window (1), the side-wall (5), and the bottom plate (7). The photocathode is deposited on the inside of the window, and makes contact with the external HV input through a metalized border (4). The grid spacers (2) and the MCP's (3) are coated with ALD. The bottom plate (7) has silk-screened silver anode 50 Ω microstrips fired on its surface (6) that penetrate a frit seal under the sidewall and connect to the digitizing electronics.

cal circuits for both signals and DC current. Atmospheric pressure transmitted through the top window and bottom anode plane compresses the 'stack' of grid spacers and microchannel plates into a rigid thin package.

A diagram of the layers of the HV divider is shown in Figure 1.

2.1. Resistive Components

Amplification in the tile is provided by a pair of microchannel-plates with 20 μm -diameter pores, arranged in a chevron configuration. The pores have a length-to-diameter ratio (L/D) of 60, making the thickness of each plate 1.2 mm. The plates are coated with a resistive layer by ALD with a target resistance of between 10 and 40 M Ω [9]. The plates are chosen within a pair to be matched in resistance within $\pm 10\%$.

To provide structural rigidity and the ability to support atmospheric pressure on the top and bottom of the package, the gaps in the vacuum volume from the cathode to the first MCP, from the first to the second MCP, and from the

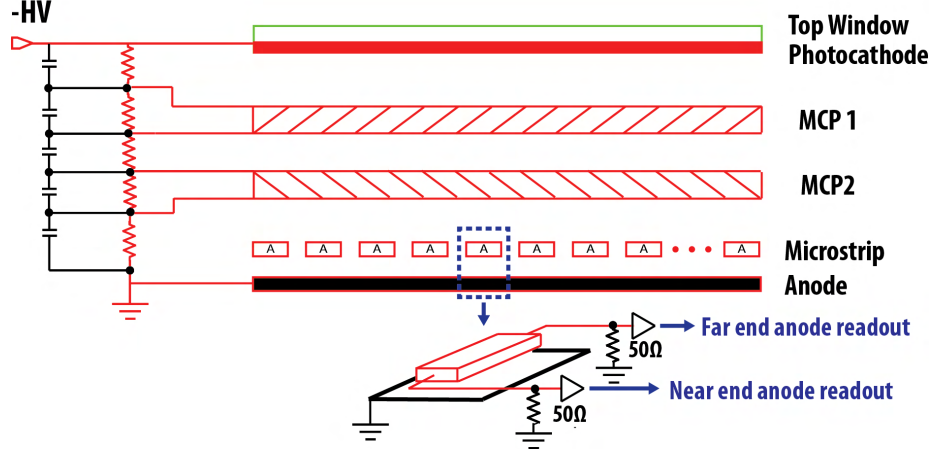


Figure 2: The equivalent electrical circuit of the tile assembly. The upper diagram shows the DC circuit. The HV voltage divider is implemented by resistive ALD coatings of the grid spacers and the MCP's. (see Figure 1).

132 second MCP to the anode, are formed by spacers consisting of thin flat glass
 133 grids. The HV resistive divider chain is completed by coating the grid spacers
 134 with a resistive layer, also by ALD, as shown in Fig. 2.

135 The parameters of the layers that make up the tile are given in Table 1 [10].
 136 A 2-mm grid spacer, shown in Figure 4, sets the height and voltage across the
 137 photocathode-MCP gap and the gap between the two MCP's. A 6.5 -mm grid
 138 spacer similarly sets the height and voltage across the gap between the bottom of
 139 the second MCP and the anode plane. The grid spacers are aligned to minimize
 140 the occluded area and to transfer the force of atmospheric pressure in columnar
 141 fashion between the top and bottom plates.

142 A 2.3 cm by 0.076 cm cut-away indentation in each crossbar in one direction
 143 in the bottom spacer allows the vacuum volumes defined by the spacer grid to
 144 communicate with each other for pumping, as shown in Figure 3.

145 We have made tests with a Nichrome coating on the grid spacers and without.
 146 Because the MCP's are metalized with Nichrome top and bottom there is no
 147 need to metalize the grid spacers at those interfaces. However metalization of

148 the top surface of the top spacer can provide a convenient method of distributing
149 HV and current across the face of the (resistive) photocathode. The silver anode
150 microstrips distribute the DC ground potential under the bottom spacer, which
151 cannot be metalized without shorting the strips.

152 *2.2. DC Current Path*

153 The DC electrical circuit of the photodetector is shown in Figure 2. High
154 voltage is applied to a Nichrome border on the underside of the window via a
155 tab that extends beyond the sidewall. The Nichrome makes contact with the
156 top grid spacer to supply current to the resistive divider through the spacers
157 and MCP's.

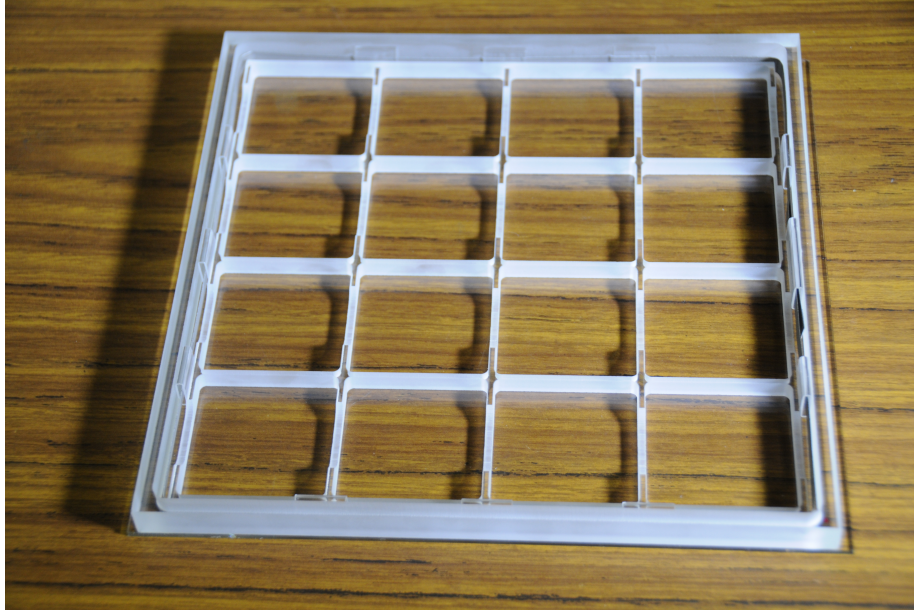


Figure 3: A partial assembly showing the ‘bottom’ spacer grid, the getter strip and its supporting glass beads, and the sidewall as they would be in the assembled tile base. The 2.3 cm by 0.076 indentations that allow the separate vacuum volumes in the tile to communicate with each other are visible as channels running from left to right on the top edges of the spacer.

Figure 5 shows the window, including the external tabs and Nichrome border that supply the input HV to the photocathode and the divider. The HV is applied to the underside of two of the tabs, and connects to the cathode through the metalization for the seal. The four metalized lines that extend into the cathode provide HV distribution to the cathode plane, complementing the distribution from the top spacer.

The internal five layers, consisting of three grid spacers and two MCP's, form a resistive voltage divider [11] that passes a nominal 100 μ A divider current from the cathode to the anode. Table 2 gives the nominal resistance and voltage drops across the divider.

The final step in the DC return path to HV ground is at each end of the anode microstrips, where individual 10K Ω resistors terminate each strip to the copper substrate sheet that forms the signal ground-plane of the microstrips

Layer	Thickness	Material	Resistive Coating	Metalization (side)
Window	2.75 mm	B33	Photocathode (bottom)	Nichrome border (bottom)
Grid Spacer 1	2.0 mm	B33	ALD-GS	None
MCP 1	1.2 mm	Micropore	ALD-MCP	Nichrome (both)
Grid Spacer 2	2.0 mm	B33	ALD-GS	None
MCP 2	1.2 mm	Micropore	ALD-MCP	Nichrome (both)
Grid Spacer 3	6.5 mm	B33	ALD-GS	None
Anode	2.75 mm	B33	N/A	Silver strips (top)

Table 1: A tabulation of the layers in the tile assembly, starting with the top window and ending with the bottom anode layer. Mechanical stability against atmospheric pressure is provided by a glass grid spacer in each of the three gaps, as listed. All components except the microchannel plates are made from B33 borosilicate glass plate [7].

171 and the HV DC return, as shown in Fig. 2.

172 2.3. The Signal Path for Fast-Risetime Pulses

173 The pulses from photons incident on the photocathode have sub-nsec rise-
174 times, with typical bandwidths for the present 20-micron pores in the 1-2 GHz
175 range. The DC HV path and the path of the fast signal pulses share the same
176 HV distribution and ground. For the signal path, however, there are two con-
177 figurations we have considered, a ‘normal’ one in which the charge of the fast
178 signals is collected and recorded from the anode microstrips inside the vacuum
179 volume, and an ‘inside-out’ geometry in which the anode is a thin metal layer
180 that serves as a DC ground, but is thin enough so that the fast signal pulses
181 capacitively couple through to strips or pads on the external side of the bottom
182 plate. These are described in turn below.

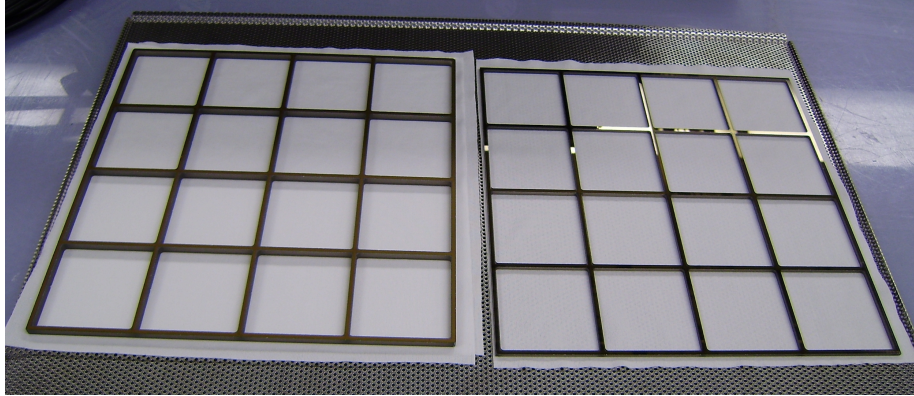


Figure 4: Two of the glass grid spacers after the resistive ALD coating has been applied. The grid spacers are cut from easily available B33 glass [7]. Mechanically, the spacers serve to transmit the compressive force of atmospheric pressure from the top to the bottom of the tube; electrically the resistive coating provides the voltage drop across each gap. Metalization of the top surface of the top spacer can serve to provide distribution of HV across the (resistive) photocathode.

183 *2.3.1. Normal Anode Configuration*

184 The signal path maintains the 50Ω impedance of the strip onto the printed
 185 circuit card containing the waveform sampling 6-channel PSEC4 ASICs [12]
 186 that digitize the signals. The thickness of the anode glass plate and the width
 187 of the strips determine the impedance of the microstrip lines [4, 13]. While
 188 the choice of impedance depends on a number of considerations, we chose a
 189 50Ω impedance for convenience in testing to match cabling and oscilloscope
 190 impedances. The choice of the anode plate thickness is application specific,
 191 with impedance, strip parameters, occupancy, weight, cost, amount of inactive

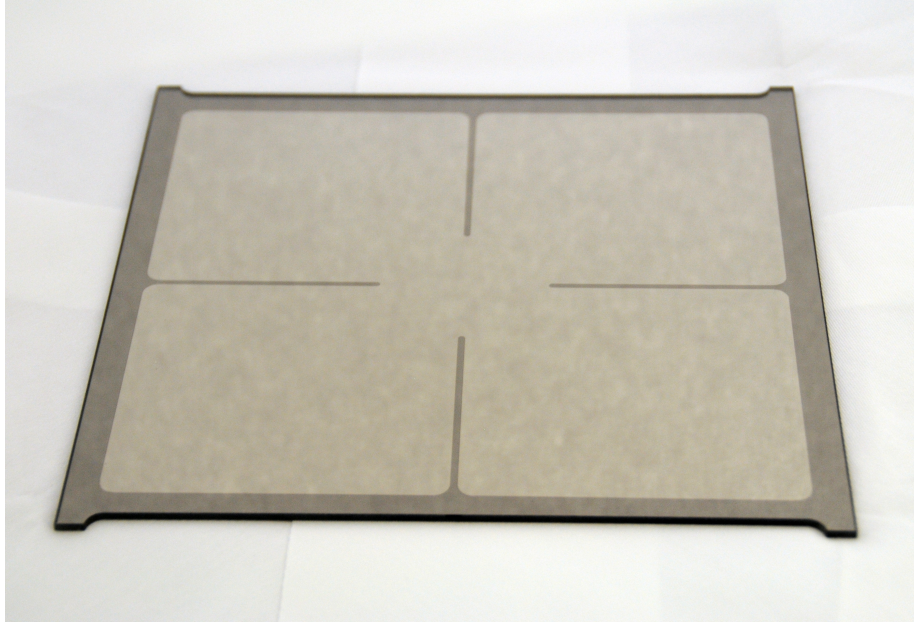


Figure 5: The glass window, showing the Nichrome border that is the ‘tie layer’ supporting the indium seal to the glass sidewall. The external tabs and the metalized border also supply the input HV to the cathode and resistive divider. The view is from the air-side (top); the Nichrome metalization for the seal and the HV distribution is visible on the vacuum-side (underneath) along the perimeter and on the four lands extending into the interior of the cathode.

Layer	Resistance	Voltage Drop
Grid Spacer 1	2 M Ω	200 V
MCP 1	10 M Ω	1000 V
Grid Spacer 2	2 M Ω	200 V
MCP 2	10 M Ω	1000 V
Grid Spacer 3	6.5 M Ω	650 V
Total	28.5 M Ω	3050 V

Table 2: The target resistances and nominal voltage drops in the internal HV divider. The divider current is set at 100 μ A, corresponding to a limit of approximately 1 μ A of current draw from signal pulses [11].

material in the path of charged particles being some of the considerations. After the plate thickness is chosen the width of the anode strips can be set so to determine the characteristic impedance. A further parameter is the gap between strips, which is vulnerable to charging in high-rate applications if electric field lines terminate on the dielectric.

Each 50 Ω stripline is impedance-matched to the PC cards that digitize the signals and that mate with the edge of the end tiles of a tile row, as shown in Fig. 6. The DC return for the divider current through the 10K Ω resistor has a much higher impedance than the 50 Ω signal path. For flexibility in testing, an easily removable connection was made using low profile Electro-Magnetic Interference (EMI) shielding gaskets [14]. Each EMI gasket strip was cut at the pitch interval into separate RF fingers and mounted on a 1/2" G10 bar to match the anode spacing. Figure 6 shows the connections between the strips on the tile and the strips on the PC card used for testing the tiles.

2.3.2. The ‘Inside-Out’ Anode

There are a number of applications, such as large collider detectors in HEP and some medical imaging cameras, that would have many particles arriving in a narrow time window and consequently high occupancies in a strip-line readout.

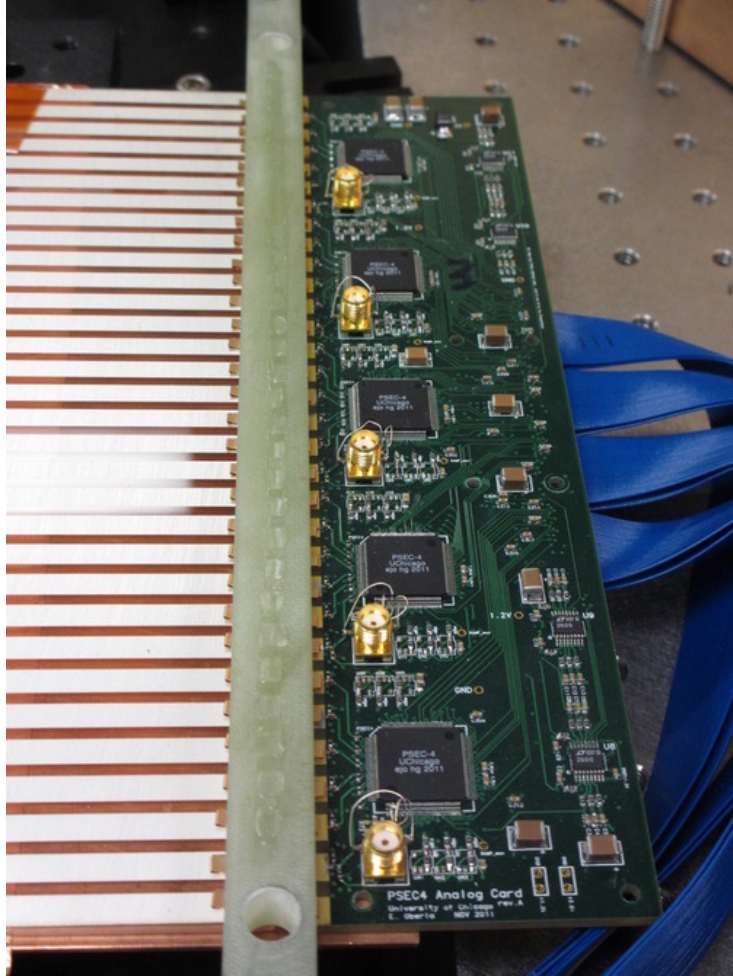


Figure 6: A picture showing the interface between the tile anodes and the readout system at the end of a row of tiles. The DC path to HV ground at the end of the microstrips is through individual $10\text{K}\Omega$ resistors on each strip to HV ground on the analog card that holds the waveform sampling ASICs. To allow easy disconnection for testing, a bar of FR4 with RF-fingers is used to bridge the gap between each of the 30 strips on the tile to the corresponding strip on the PC card.

210 These applications would benefit from a 2-dimensional ‘pad’ readout rather than
211 a 1-dimensional stripline geometry.

212 The fast risetime of the signal pulses from the MCP amplification chain
213 provides a mechanism to extract the signals from the vacuum volume by ca-
214 pacitively coupling through the glass anode bottom plane. In this ‘inside-out’
215 implementation, a uniform metal layer thinner than a skin-depth at frequencies
216 characteristic of the MCP risetime is deposited on the inner (vacuum-side) side
217 of the anode bottom glass plate, replacing the microstrips. This layer provides
218 the ground return for the DC HV current. The outer (air-side) side of the anode
219 plate supports the readout pattern deposited by metalization, typically in pads
220 or strips. This layer can then be connected to the electronics and additional
221 grounds as necessary.

222 **3. Implementation in the LAPPDTM Package**

223 The LAPPDTM design integrates the mechanical structure with both the
224 high frequency signal path and the HV DC current path into a single economical
225 structure. The advantage of the integrated design is the construction is planar,
226 with all electrical connections lying in the same plane as the thin form-factor
227 detector module itself. This allows a ‘tiling’ of large areas with a higher filling
228 factor than would be possible with individual modules with edge-readout. We
229 give details of the implementation below.

230 *3.1. Mechanical Dimensions*

231 The tile assembly is a flat glass package with transverse dimensions of 229.1
232 mm in the strip direction by 220 mm transverse. The active area is 203 mm
233 by 203 mm (8” by 8”). The current prototype grid spacers occlude 16% of the
234 active area; this will be reduced in future designs after more experience with
235 this first-generation simple implementation.

236 A mockup of an assembled glass module, made with prototype glass parts
237 but without a photocathode or vacuum seal, is shown in Figure 7. Multi-
238 ple modules can be integrated into a ‘supermodule’, sharing the RF-strip-line

239 readout mounted on the ‘Tray’ that also supports the electronics, as shown in
 240 Figure 8 [4].

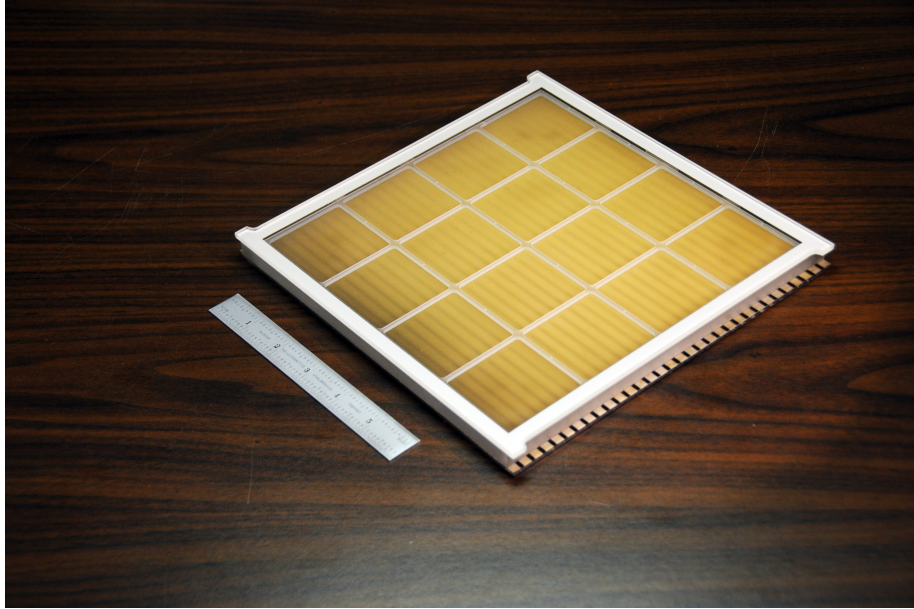


Figure 7: An 8”-square (20 cm-by-20 cm) LAPPDTM module (‘tile’). The tiles are hermetically sealed vacuum tubes that provide the photocathode and MCP-based amplification chain. The upper layer of the micro-strip RF transmission lines that form the anode are on the internal surface of the bottom plate of the tile; the ground plane of the transmission line is the upper surface of the supporting ‘Tray’, shown in Figure 8. The thin format and modular nature of the photodetector allow application-specific optimization.

241 The tile is made from glass layers stacked to form a rigid structure when
 242 compressed by atmospheric pressure. The vacuum volume is enclosed by the
 243 2.75 mm-thick top window, a standard plate glass thickness. The photocathode
 244 is on the bottom surface of the window, facing the top of the upper MCP (see
 245 Fig. 1). The anode plate with silver microstrips on its top surface, serves as the
 246 bottom of the vacuum volume, and is also 2.75 mm-thick. A rectangular border
 247 of 5.08 mm (0.200”) width, cut from a standard thickness glass plate, forms the

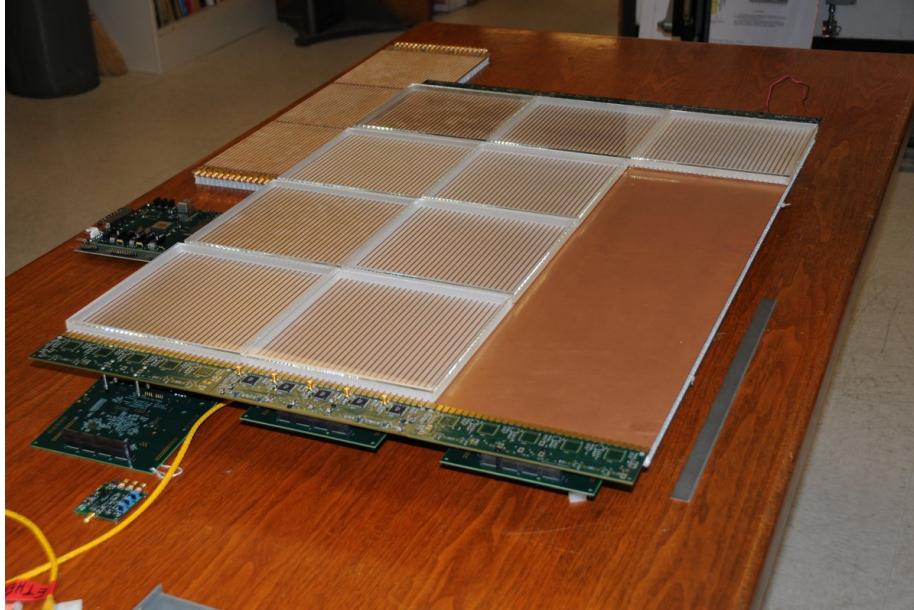


Figure 8: A ‘supermodule’ consisting of twelve 8”-square LAPPDTM modules (‘tiles’) mounted on a ‘tray’ that provides the ground plane for the anode microstrips and the support for the digitizing electronics at each end. Each row of 4 tiles shares the same anode strips in series, as described in Ref. [4].

248 sidewall of the volume.

249 The sidewall is sealed to the anode plate over the microstrips with a glass
250 frit seal. The metal microstrips extend beyond the sidewall so that contact can
251 be made with neighboring tiles [4] or the digitization printed circuit cards at
252 the end of a tile-row [12].

253 4. Performance of the HV Divider

254 The proposal to use ALD coatings on the grid spacers and MCP’s to deter-
255 mine the amplification and transport voltages had unknown risks at the outset
256 of the LAPPD program. In particular we are relying on the stability of the
257 coatings under a large mechanical pressure. Atmospheric pressure corresponds
258 to almost 1200 lbs on the top and bottom plates. The pressure on the MCP

surfaces is magnified by the ratio of areas of the grid spacer to the total area, approximately a factor of 10. The surfaces of the MCP's consist of glass capillaries with $\sim 65\%$ open area, and have both metal electrode material and ALD secondary-emitting material; the surfaces of the grid spacers have a grid-specific ALD resistive coating. How these interfaces behave under pressure, with temperature, and over time is not tractable to calculation; we have consequently embarked on a series of measurements of the stability of the HV divider assembly under HV and pressure. Several of the test facilities are described in turn below.

4.1. Test Facilities

Section 4.1.1 describes a custom test facility, the Spacer Station (ISS) used to make DC measurements of current and voltage. A second test facility, the 'Demountable Tile', consisting of an actively-pumped glass-body tile mechanical assembly with an O-ring top seal, is used to make measurements of fast pulses at resolutions down to 5 psec, as described in Section 4.1.2.

4.1.1. The Spacer Station (ISS)

To measure the resistance of the grid spacers and MCP plates versus pressure, temperature, and over time, a simple flat square vacuum vessel with a flexible lid consisting of an aluminum foil incapable of withstanding atmospheric pressure was constructed. The window provides the same (atmospheric) pressure on the component stack as the glass window of the sealed tile. Figure 9 shows the ISS open to air with a single grid spacer inside. The copper plate to the right of the ISS provides HV contact to the layers being measured; the ISS frame is the DC ground. Single, multiple, or a full stack of the component layers (grid spacer and MCP) can be measured using suitable non-conducting spacers above the copper plate.

4.1.2. The Demountable Tile

In order to test the time and position response of the photodetectors as a system we have constructed a facility [15] of which the key components are a

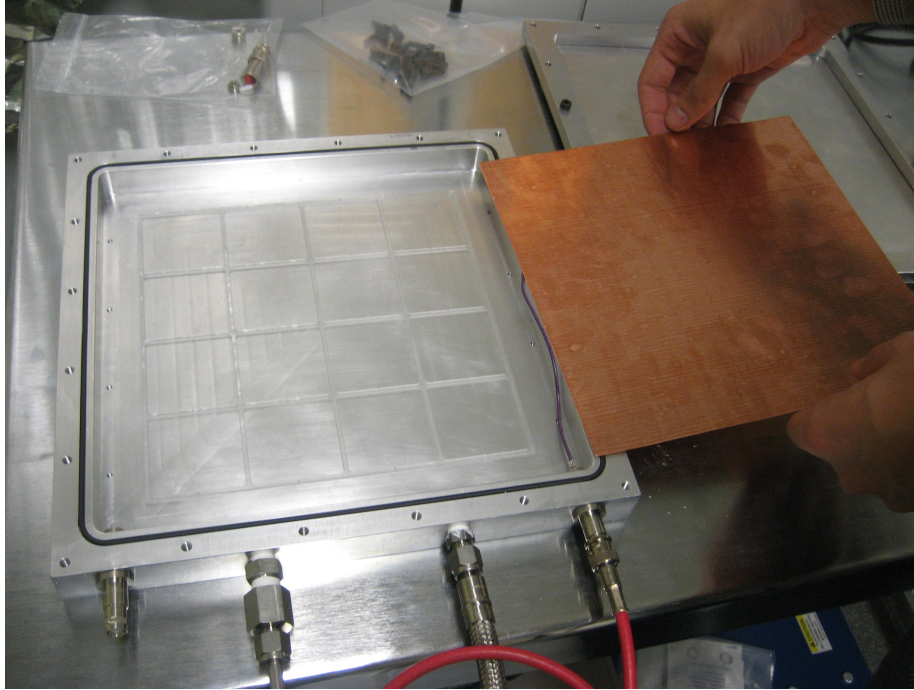


Figure 9: The spacer station (ISS) used to measure resistances of individual grid spacers, MCP's, and the complete divider. A grid spacer is shown in the vacuum volume; the copper plate being held on the right is an electrode that supplies the HV to the piece being measured. A thin insulating layer separates the copper HV electrode from the 2.75-mm-thick top window, which is thin enough that atmospheric pressure deflects it until stopped by the internal stack of MCP's and grid spacers, compressing the divider.

288 pulsed Ti:Sapphire laser with a pulse width ~ 100 fsec, and a data-acquisition
 289 system with 60 channels of 10-15 GS/sec waveform sampling readout, shown
 290 in Figure 10. The Demountable Tile is constructed with the anode frit-sealed
 291 to the sidewall and the internal HV divider as in the LAPPDTM, but has
 292 a removable window sealed with an O-ring so that MCP plates can be easily
 293 inserted and removed for rapid testing. The tile consequently has to be actively
 294 pumped, and has an air-stable aluminum cathode.

295 The HV control system for the Demountable Tile Test Facility allows for
 296 measuring voltage and current under computer control [15], and similarly mea-
 297 suring the stability of the gain and spatial response over the face of the tile [16].
 298

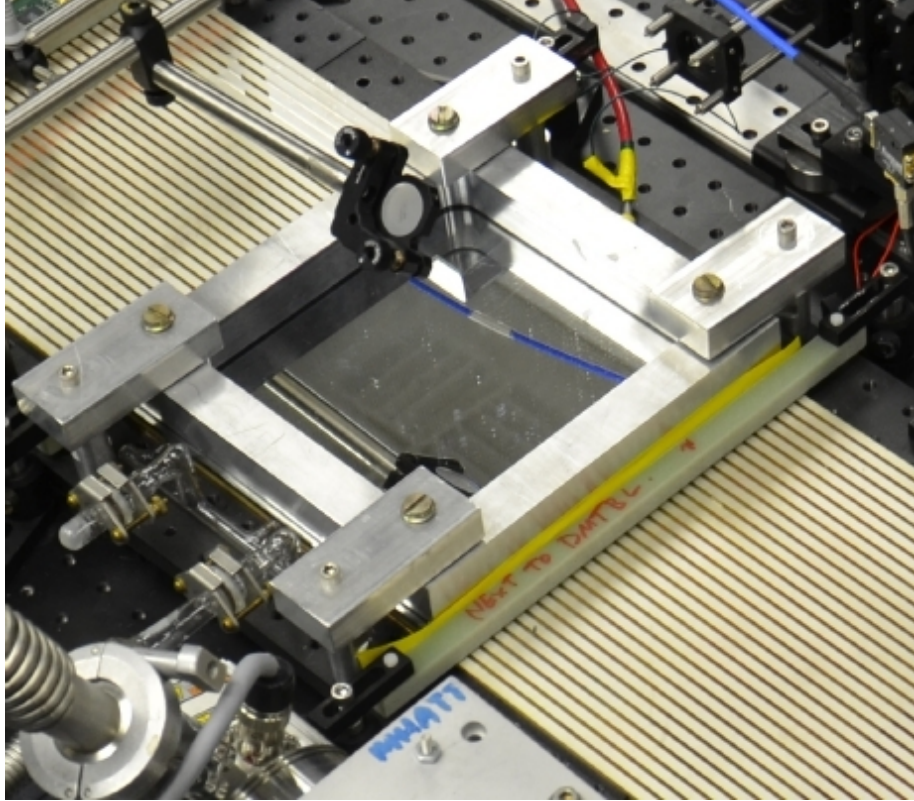


Figure 10: The Demountable Tile test setup, consisting of glass tile of the LAPPDTM design constructed with the LAPPDTM hermetic package and internal divider, but with a removable window sealed with an O-ring. The tile consequently has to be actively pumped, and, as a bialkali anode cannot survive in air, has an aluminum cathode. However the HV divider and signal circuit are the same as in the sealed tile. The tile is shown sitting on a 4-tile anode readout ‘Tray’, which is equipped with 60 channels (30 strips on each end) of 10-15 GS/sec waveform sampling PSEC-4 ASICs.

299 4.2. Current-vs-Voltage (I-V) Curves

300 One concern about using ALD-coated elements as a HV divider is the possi-
 301 ble non-linear or non-reproducible behavior as a function of voltage. Figure 11
 302 shows the measured I-V curve using the ISS facility. The behavior is linear, and
 303 demonstrates little hysteresis.

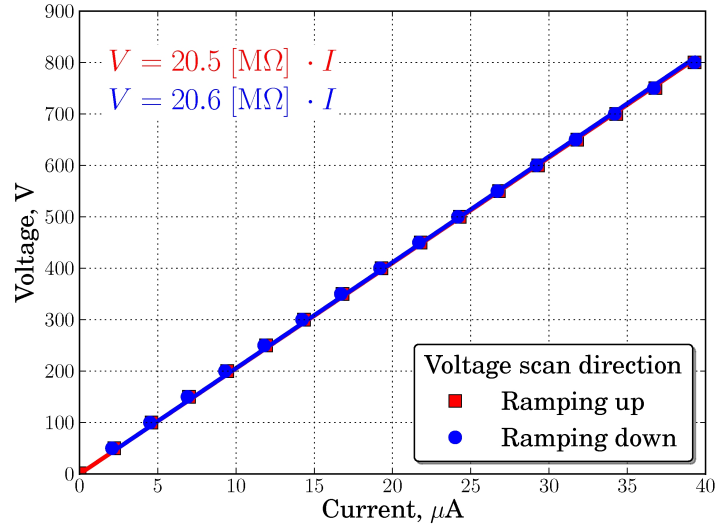


Figure 11: The current-vs-voltage (I-V) data for the ALD-based HV divider, as measured in the ISS test facility. The voltage is measured both ramping up and ramping down increased (red, squares) vs decreased (blue, circles). The slope gives the effective resistance of the multi-layer divider.

304 4.3. Thermal Coefficient

305 The temperature dependence of the divider resistance is of concern due to
 306 the vulnerability of MCP-based photodetectors to thermal run-away [17]. The
 307 divider resistance depends on the thermal coefficients of the ALD-coatings of
 308 the grid-spacers and MCP's. The resistivity of the coatings on the grid spacers
 309 is different from that for the MCP's, as the effective conducting areas are so
 310 different. At present the three grid spacers are coated in the same batch, so the

311 difference in resistance is determined solely by the difference in the conduction
 312 path length of the thicker grid spacer from that of the other two (see Table 1).
 313 Figure 12 shows the resistance of the HV divider as a function of temperature,
 314 measured in the ISS.

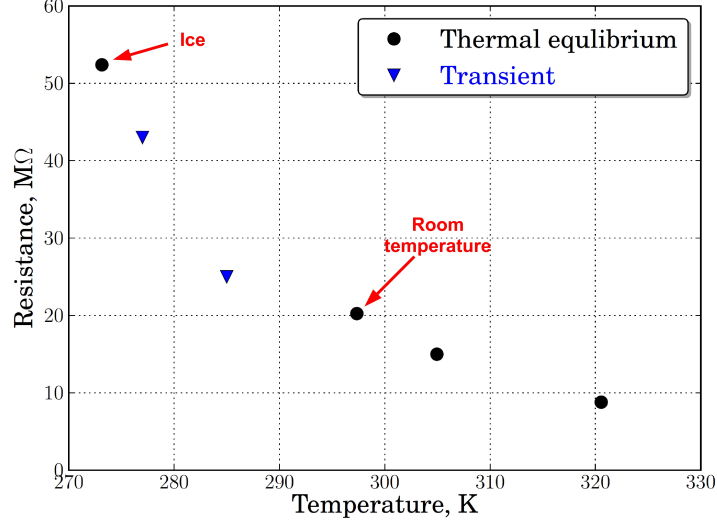


Figure 12: The resistance of the HV divider as a function of temperature. The measurements between room temperature and the temperature of ice were measured by necessity ‘on the fly’, rather than in thermal equilibrium, a possible explanation of the apparent offset from the curve.

315 4.4. Pressure Dependence

316 The contacts between the grid spacers and the MCP’s are complex electri-
 317 cally and mechanically [18]. The Spacer Station (ISS) was constructed with
 318 a thin foil top ‘window’ specifically to measure the contact resistances versus
 319 pressure. The pressure is varied by control of the vacuum inside the ISS through
 320 a needle valve to the pump. A curve of resistance vs the pressure on the layers
 321 of the HV divider (lbs/in²) is shown in Figure 13. The drop in resistance of
 322 approximately 20% at low pressure is presumably due to changes in contact. A

323 small amount of hysteresis is observed; however in an operating evacuated tile
 324 the pressure on the stack is stable, with only minor variations due to changes
 325 in atmospheric pressure or temperature.

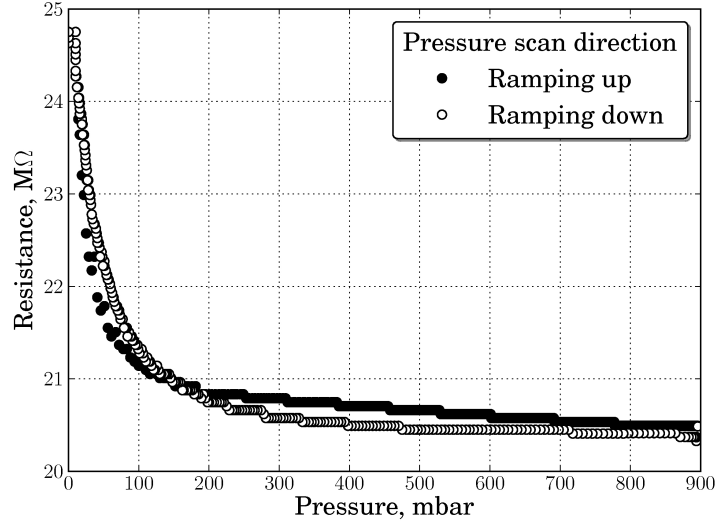


Figure 13: The resistance of the HV divider as a function of the pressure compressing the divider stack. The pressure is varied by using the differential between atmospheric pressure on one side of the thin foil window at the top of the ISS and the partial vacuum inside the volume. The pressure in the ISS is controlled by pumping through a needle valve. Note the suppressed zero on the ordinate.

326 4.5. Long-term Stability

327 The large pressure (> 1000 lbs) on the HV divider transmitted through the
 328 thin glass top window and bottom plate is also cause for concern about the
 329 long-term stability of the electrical contacts between the layers that constitute
 330 the divider. The mechanical and electrical stability of the interface are subject
 331 to changes due to pressure, electro-chemistry, and temperature, as well as a
 332 possible slow creep of a component or layer under the pressure. Over the course

333 of 11 months under vacuum, a stack of two MCP's and 3 grid spacers the
334 Demountable Tile has remained stable in resistance, gain, and uniformity, giving
335 us confidence in the mechanical design.

336 5. Conclusions

337 The use of ALD for functionalizing glass capillaries and glass grid spacers
338 enables a modular compact design of a thin planar photodetector with an in-
339 ternal HV divider. The LAPPDTM module is simple, consisting of eight parts,
340 all made of glass, and a simple getter assembly. The amplification section con-
341 sists of two 203 mm-by-203 mm MCP's. The HV divider is formed by applying
342 resistive coatings to the grid spacer in each of the three gaps: between the pho-
343 tothode and MCP1, between MCP1 and MCP2, and between MCP2 and the
344 anode microstrip transmission lines.

345 The sealed module sits flat on a ground plane that is shared with neighboring
346 modules; there are no connecting pins on the back side. The HV is applied to an
347 external metalized tab that connects to the metal top seal between the window
348 and the glass sidewall. The DC ground is provided by the anode ground plane
349 of microstrips, which are deposited on the top surface of the glass bottom plate
350 of the hermetic package, and extend through the seal to outside the vacuum
351 volume. The anode microstrips can be connected in series to form a continuous
352 anode up to 90 cm long, with the DC ground return and ASIC readout on the
353 ends of the outer-most modules [4].

354 Measurements of current vs voltage in the HV divider have been made in
355 a custom test setup and in the module glass body on a 90-cm anode. The
356 measurements in the test setup have been made as a function of the pressure on
357 the divider, controlled by varying the vacuum in the module. Measurements of
358 the temperature dependence and stability are also presented. An 11-month test
359 under vacuum gives us confidence in the long-term stability of this relatively
360 simple integrated electro-mechanical design.

361 **6. Acknowledgments**

362 We thank our colleagues in the Large Area Psec Photodetector (LAPPD)
363 Collaboration for their contributions and support. Special thanks are due to A.
364 O'Mahony (Incom) and Neal Sullivan (Arradance) for their essential work on
365 ALD coatings for the components of the internal stack. Thanks are due to R.
366 G. Wagner (ANL) for technical support; D. Walters, and J. Williams (ANL) for
367 metalization of the windows and vacuum expertise; and H. Wen and H. Gibson
368 (ANL) for laser and electronics support at the APS testing lab. We are deeply
369 grateful to E. Hahn (Fermilab) for meticulous metalization of the MCP's, and P.
370 Murat (Fermilab) for support. R. Metz (UC) provided expert machining of test
371 setups and glass parts. M. Heintz (UC) supplied crucial technical and computer
372 systems support. We thank Q. Guo (UC), Chian Liu (ANL) and H. Clausing
373 (H. Clausing, Inc) for expert advice and large amounts of time teaching us about
374 cleaning and metalization of glass. We also thank our superb glass vendors P.
375 Jaynes (CatI Glass, Inc) and P. Seegebrecht (Webcorr) for metalization and
376 glass

377 The activities at Argonne National Laboratory were supported by the U. S.
378 Department of Energy, Office of Science, Office of Basic Energy Sciences and
379 Office of High Energy Physics under contract DE-AC02-06CH11357, and at
380 the University of Chicago by the Department of Energy under DE-SC-0008172,
381 the National Science Foundation under grant PHY-1066014, and the Driskill
382 Foundation.

References

- [1] The original LAPPD institutions include ANL, Arradance Inc., the Univ. of Chicago, Fermilab, the Univ. of Hawaii, Muons, Inc., SLAC, SSL/UCB, and Synkera Corporation. More detail can be found at <http://psec.uchicago.edu/>.
- [2] J.L. Wiza, Micro-channel Plate Detectors. Nucl. Instr. Meth. 162, p567; 1979
- [3] E. Oberla, Ph.D thesis, in preparation. We thank H. Nicholson for the original suggestion of using large-area planar detectors for water Cherenkov neutrino detectors, and for the OTPC name.
- [4] H. Grabas, R. Obaid, E. Oberla, H. Frisch, J.-F. Genat, R. Northrop, F. Tang, D. McGinnis, B. Adams, M. Wetstein, *RF Strip-Line Anodes for Psec Large-Area MCP-based Photodetectors*. Nucl. Instr. Meth. A71, p124; 2013
- [5] The glass capillary substrates are produced by Incom Inc. Charlton Mass. See <http://www.incomusa.com/>.
- [6] S. M. George, *Atomic Layer Deposition: An Overview*; Chemical Reviews 2010, 110, (1), 111-131;
J. W. Elam, D. Routkevitch, and S. M. George, *Properties of ZnO/Al₂O₃ Alloy Films Grown Using Atomic Layer Deposition Techniques*; Journal of the Electrochemical Society 2003, 150, (6), G339-G347;
D. R. Beaulieu, D. Gorelikov, H. Klotzsch, P. de Rouffignac, K. Saadatmand, K. Stenton, N. Sullivan, and A. S. Tremsin, *Plastic microchannel plates with nano-engineered films*; Nucl. Instr. Meth. A633, S59-S61 (2011);
O.H.W. Siegmund, J.B. McPhate, S.R. Jelinsky, J.V. Vallerga, A.S. Tremsin, R. Hemphill, H.J. Frisch, R.G. Wagner, J. Elam, and A. Mane, *Development of Large Area Photon Counting Detectors Optimized for Cherenkov Light Imaging with High Temporal and sub-mm Spatial Resolution*; NSS/MIC 2011 IEEE, p2063 (Oct., 2011).

- 411 [7] http://psec.uchicago.edu/glass/borofloat_33.e.pdf#page=28; The dielec-
 412 tric constant is 4.6 and the loss tangent is 37×10^{-4} , both measured at
 413 25C and 1 MHz.
- 414 [8] Ferro Corp., 251 Wylie Ave., Washington PA 15301. We are grateful to E.
 415 Axtel for extensive assistance with selecting the silver ink for silk-screening
 416 the anode microstrips.
- 417 [9] A. U. Mane, W. M. Tong, A. D. Brodie, M. A. McCord, and J. W. Elam,
 418 *Atomic Layer Deposition of Nanostructured Tunable Resistance Coatings:*
 419 *Growth, Characterization, and Electrical Properties*, ECS Transactions, 64
 420 (9) 3-14 (2014);
 421 A. U. Mane and J. W. Elam, *Atomic Layer Deposition of W:Al₂O₃*
 422 *Nanocomposite Films with Tunable Resistivity*, Chem. Vap. Deposition, 19,
 423 186-193, (2013)
- 424 [10] The tabulated values are those in current use. They can be changed to
 425 optimize the voltages across the respective gaps for specific performance
 426 goals. The total thickness depends on the height of the sidewall, which also
 427 can be optimized for different applications.
- 428 [11] *Photomultiplier Tubes: Principles and Applications*, S-O Flyckt and C.
 429 Marmonier; Photonis Brive, France, Sept. 2002
- 430 [12] E. Oberla, H. Grabas, J.-F. Genat, H. Frisch, K. Nishimura, G. S.
 431 Varner, *A 15 GSa/s, 1.5 GHz Bandwidth Waveform Digitizing ASIC*,
 432 Nucl.Instrum.Meth. A735 (2014) 452-461.
- 433 [13] For an excellent discussion of transmission lines, see E. Bogatin, *Signal*
 434 *Integrity Simplified*, Prentice Hall Professional Technical Reference, 2004.
 435 Chapter 10 is especially clear on cross-talk in striplines.
- 436 [14] Leader Tech part number 12-60LPAH-BD-16; Laird Technologies, Item 97-
 437 115

- 438 [15] B. Adams, M. Chollet, A. Elagin, R. Obaid, E. Oberla, A. Vostrikov,
439 P. Webster, M. Wetstein; *A Test-Facility for Large-area Microchannel Plate*
440 *Detector Assemblies Using a Pulsed sub-Picosecond Laser*, Rev. Sci. In-
441 strum. 84, 061301 (2013)
- 442 [16] B. Adams, A. Elagin, M. Wetstein et al.; *Measurements of the Gain, Time*
443 *Resolution, and Spatial Resolution of a 2020 cm² MCP-based Picosecond*
444 *Photo-detector*, Nucl. Instrum. Meth. A732 (2013)
- 445 [17] C. W. Carlson and J. P. McFadden *Design and Application of Imaging*
446 *Plasma Instruments*, in *Measurement Techniques in Space Plasmas: Parti-*
447 *cles*, R. F. Pfaff, J.E. Borovsky, and D. T. Young eds.; American Geophys-
448 ical Union pub. (1998)
- 449 [18] The measurements presented here are made with MCP's that have the
450 electrode surface 'under' the ALD resistive and emissive coatings. The other
451 option, 'over', has the electrode on top of the ALD coatings. Both options
452 have their merits and drawbacks.